



1 **Wave spectral shapes in the coastal waters based on measured data off Karwar, west coast of**
2 **India**

3 Anjali Nair M, Sanil Kumar V

4

5 Ocean Engineering Division

6 Council of Scientific & Industrial Research-National Institute of Oceanography

7 Dona Paula 403 004, Goa India

8

9 *Correspondence to email:sanil@nio.org Tel: 0091 832 2450 327

10

11

12 **Abstract**

13

14 Understanding of the wave spectral shapes is of primary importance for the design of
15 marine facilities. In this paper, the wave spectra collected from January 2011 to December 2015 in
16 the coastal waters are examined to know the temporal variations in the wave spectral shape. For
17 31.15% of the time, peak frequency is between 0.08 and 0.10 Hz and the significant wave height is
18 also relatively high (~ 1.55 m) for waves in this class. The slope of the high-frequency tail of the
19 monthly average wave spectra is high during the Indian summer monsoon period (June-September)
20 compared to other months and it increases with increase in significant wave height. There is no
21 much interannual variation in slope for swell dominated spectra during the monsoon, while in the
22 non-monsoon period when wind-seas have much influence, the slope varies significantly. Since the
23 high-frequency slope of the wave spectrum is within the range 3-4 during the monsoon period,
24 Donelan spectrum shows better fit for the wave spectra in monsoon months compared to other
25 months.

26

27 **Key Words:** Ocean surface waves, wind waves, Arabian Sea, wave spectrum, high-frequency tail

28



29 1. Introduction

30

31 Information on wave spectral shapes are required for designing the marine structures
32 (Chakrabarti, 2005) and almost all the wave computations are based on the wave spectral function
33 (Yuan and Huang, 2012). The growth of waves and the spectral shape is due to the complex ocean-
34 atmosphere interactions, while the physics of air-sea interaction is not completely understood
35 (Cavaleri et al., 2012). The shape of the wave spectrum depends on the factors governing the wave
36 growth and decay and a number of spectral shapes are proposed in the past for different sea states
37 (see Chakrabarti, 2005 for a review). The spectral shape is maintained by nonlinear transfer of
38 energy through nonlinear four-wave interactions (quadruplet interactions) and white-capping
39 (Gunson and Symonds, 2014). The momentum flux between the ocean and atmosphere govern the
40 high-frequency wave components (Cavaleri et al., 2012). According to Philips, the equilibrium
41 ranges for low-frequency and high-frequency region is proportional to f^5 and f^4 (where f is the
42 frequency) respectively. Several field studies made since JONSWAP reveal an analytical form for
43 wave spectra with the spectral tail proportional to f^4 (Toba, 1973; Kawai et al., 1977; Kahma,
44 1981; Forristall, 1981; Donelan et al., 1985). Usually there is a predominance of swell fields in
45 large oceanic areas, which is due to remote storms (Chen et al., 2002; Hwang et al., 2011; Semedo
46 et al., 2011). The exponent used in the expression for the frequency tail has different values (see
47 Siadatmousavi et al., 2012 for a brief review). For shallow water, Kitaigorodskii et al. (1975)
48 suggested f^{-3} tail, Liu (1989) suggested f^{-4} for growing young wind-seas and f^{-3} for fully developed
49 wave spectra. Badulin et al. (2007) suggested f^4 for frequencies where nonlinear interactions are
50 dominant. The study carried out at Lake George by Young and Babanin (2006) revealed that in the
51 frequency range $5f_p < f < 10f_p$, the average value of the exponent 'n' of f^n is close to 4. Whereas,
52 some studies in real sea conditions indicate that high-frequency shape of f^4 applies up to few times
53 peak frequency (f_p) and then decays faster with frequency. The spectra for coastlines in Currituck
54 Sound with short fetch condition showed a decay closer to f^5 when f is greater than two or three
55 times peak frequency (Long and Resio, 2007). Gagnaire-Renou et al. (2010) found that the energy
56 input from wind and dissipation due to white-capping have a significant influence on the high-
57 frequency tail of the spectrum.

58

59 The physical processes in the north Indian Ocean have a distinct seasonal cycle (Shetye et
60 al., 1985) and the surface wind-wave field is no exception (Sanil Kumar et al., 2012). In the eastern



61 AS, significant wave height (H_{m0}) up to 6 m is measured in the monsoon period (June to
62 September), and during rest of the period, H_{m0} is normally less than 1.5 m (Sanil Kumar and
63 Anand, 2004). Sanil Kumar et al. (2014) observed that in the eastern AS, the wave spectral shapes
64 are different at two locations within 350 km distance, even though the difference in the integrated
65 parameter like H_{m0} is marginal. Dora and Sanil Kumar (2015) observed that waves at 7-m water
66 depth in the nearshore zone off Karwar are high energy waves in the monsoon and low to moderate
67 waves in the non-monsoon period. Dora and Sanil Kumar (2015) study shows similar contribution
68 of wind-seas and swells during the pre-monsoon (February to May), while swells dominate the
69 wind-sea in the post-monsoon (October to January) and the monsoon period. Earlier studies
70 indicate that the spectral tail of the high-frequency part shows large variation and its variation with
71 seasons are not known. Similarly, the shape of the parametric spectra are also different and hence it
72 is important to identify the spectral shapes based on the measured data covering all the seasons and
73 different years.

74

75 The previous discussion shows that there is a strong inspiration to study the high-frequency
76 tail of the wave spectrum. For the present study, we used the measured wave spectral data at 15-m
77 water depth off Karwar, west coast of India over 5 years during 2011 to 2015 and evaluated the
78 nearshore wave spectral shapes in different months. This study addresses two main questions: (1)
79 How the high-frequency tail of the wave spectrum varies in different months ? (2) What are the
80 spectral parameters for the best-fit theoretical spectra ? This paper is organized as follows: the
81 study area is introduced in section 2, details of data used and methodology in section 3. Section 4
82 presents the results of the study and the conclusions are given in section 5.

83

84 2. Study area

85

86 The coastline at Karwar is 24° inclined to the west from the north and the 20 m depth
87 contour is inclined 29° to the west. Hence, large waves in the nearshore will have direction close to
88 241° since waves get aligned with the depth contour due to refraction. At 10, 30 and 75 km distance
89 from Karwar, the depth contours of 20, 50 and 100 m are present (Fig. 1). The study region is
90 under the seasonally reversing monsoon winds, with winds from the northeast during the post-
91 monsoon and from the southwest during the monsoon period. The monsoon winds are strong and
92 the total seasonal rainfall is 280 cm. The average monthly sea level at Karwar varies from 1.06 m



93 (in September) to 1.3 m (in January) and the average tidal range is 1.58 m during spring tide and
94 0.72 m during neap tide (Sanil Kumar et al., 2012).

95

96 3. Materials and methods

97

98 The waves off Karwar (14° 49' 56" N and 74° 6' 4" E) are measured using the directional
99 waverider buoy (Barstow and Kollstad, 1991). Measurements are carried out from 1 January 2011
100 to 31 December 2015. The data for every 30 minutes from the continuous records at 1.28 Hz are
101 processed as one record. From the time series data, the wave spectrum is obtained through fast
102 Fourier transform (FFT). Bulk wave parameters; significant wave height (H_{m0}) which equals
103 $4\sqrt{m_0}$ and mean wave period (T_{m02}) based on second order moment, which equals $\sqrt{m_0/m_2}$ are
104 obtained from the spectral moments. Where m_n is the n^{th} order spectral moment ($m_n = \int_0^\infty f^n S(f) df$,
105 $n=0$ and 2), $S(f)$ is the spectral energy density at frequency f . The spectral peak period (T_p) is
106 estimated from the wave spectrum and the peak wave direction (D_p) is estimated based on circular
107 moments (Kuik et al., 1988). The wind-seas and swells are separated through the method described
108 by Portilla et al. (2009) and the wind-sea and the swell parameters are computed by integrating over
109 the respective spectral parts. Measurements reported here are in Coordinated Universal Time
110 (UTC), which is 05:30 h behind the local time. U is the wind speed at 10-m height obtained from
111 reanalysis data of zonal and meridional components at 6 hourly intervals from NCEP / NCAR
112 (Kalnay et al., 1996).

113

114 Wave spectrum continues to develop through non-linear wave-wave interactions even for
115 very long times and distances. Hence, most of the wave spectrum is not fully developed and cannot
116 be represented by Pierson-Moskowitz (PM) spectrum (Pierson and Moskowitz, 1964). Accordingly,
117 an additional factor was added to the PM spectrum in order to improve the fit to the measured
118 spectrum. The JONSWAP spectrum (Hasselmann et al., 1973) is thus a PM spectrum multiplied by
119 an extra peak enhancement factor γ . The high-frequency tail of the JONSWAP spectrum decays in
120 a form proportional to f^{-5} . A number of studies reported that high-frequency decay is by a form
121 proportional to f^{-4} . Modified JONSWAP spectrum including Toba's formulation of saturation range
122 was proposed by Donelan et al. (1985). The JONSWAP and Donelan spectrum used in the study
123 are given in eqns. (1) and (2).



$$124 \quad S(f) = \frac{\alpha g^2}{(2\pi)^4 f^5} \exp \left[-\frac{5}{4} \left(\frac{f}{f_p} \right)^{-4} \right] \gamma \exp \left[-\frac{(f-f_p)^2}{2\sigma^2 f_p^2} \right] \quad \dots\dots\dots (1)$$

$$125 \quad S(f) = \frac{\alpha g^2}{(2\pi)^4 f^4 f_p} \exp \left[-\left(\frac{f}{f_p} \right)^{-4} \right] \gamma \exp \left[-\frac{(f-f_p)^2}{2\sigma^2 f_p^2} \right] \quad \dots\dots\dots (2)$$

126 Where γ is the peak enhancement parameter; α is Philip's constant; f is the wave frequency; g is the
 127 gravitational acceleration and σ is the width parameter.

$$128 \quad \sigma = \begin{cases} 0.07, & f < f_p \\ 0.09, & f \geq f_p \end{cases}$$

129
 130

131 **4. Results and discussions**

132

133 **4.1 Bulk wave parameters**

134

135 The persistent monsoon winds generate choppy seas with average wave heights of 2 m and
 136 mean wave period of 6.5 s. In the monsoon, the observed waves had a maximum H_{m0} of about 5 m,
 137 with H_{m0} of 2-2.5 m more common and the maximum H_{m0} measured is on 21 June 2015 17:30 UTC
 138 (Fig. 2a). Mean wave periods (T_{m02}) at the measurement location ranged from 4-8 s. Wave direction
 139 during monsoon is predominantly from the west due to refraction towards the coast. The fluctuation
 140 in H_{m0} due to the southwest monsoon is seen in all the years (Fig. 2a). High waves ($H_{m0} > 2$ m)
 141 during 27-29 November 2011 is due to the deep depression ARB04 formed in the Arabian Sea
 142 (AS). During the study period, the annual average H_{m0} is same (~1.1 m) in all the years (Table 1).
 143 In 2013, the data during August could not be collected and hence resulted in lower annual average
 144 H_{m0} . Over the 5 years, small waves ($H_{m0} < 1$ m) account for a large proportion (63.94%) of
 145 measured data and only during 0.16% of the time, H_{m0} exceeded 4 m (Table 2). The 25th and 75th
 146 percentiles of the H_{m0} distribution over the entire analysis period are 0.6 and 1.4 m.

147

148 Small waves ($H_{m0} < 1$ m) are with the mean period in a large range (2.7-10.5 s), whereas
 149 high waves ($H_{m0} > 3$ m) have mean wave period in a narrow range (6.1-9.3 s) (Table 2). For waves
 150 with H_{m0} more than 3 m, the T_p never exceeded 14.3 s and for waves with H_{m0} less than 1 m, T_p



151 up to 22.2 s are observed (Fig. 2c) and the long period swells (14-20 s) are with $H_{m0} < 2.5$ m.
152 Around 7% of the time during 2011-2015, waves have peak period more than 16.7 s (Table 3).
153 Peak frequency between 0.08 and 0.10 Hz, equivalent to a peak wave period of 10 - 12.5 s is
154 observed in 31.15% of the time and the H_{m0} is also relatively high (~ 1.55 m) for waves in this
155 class. During the annual cycle, the wave climate is dominated by low waves ($0.5 > H_{m0} > 1$ m),
156 intermediate-period ($T_p \sim 10$ -16s) south-westerly swell. Waves from the northwest are with T_p less
157 than 8 s (Fig. 3).

158

159 The wave roses during 2011-2015 indicate that around 38% of the time during the period
160 2011 to 2015, the predominant wave direction is SSW (225°) with long period (14 - 18s) and
161 intermediate period (10 - 14s) waves (Fig. 3). A small percentage of long-period waves having H_{m0}
162 more than 1m are observed from the same direction in which more than 80% are swells (Fig. 3c).
163 Intermediate period waves observed having H_{m0} less than 1m, contain 20 - 60% of swells. Around
164 10-15% of the waves observed during the period are from the west, which includes intermediate
165 and short period waves with H_{m0} varying from 1.5 to 3m. These intermediate period waves from
166 west having H_{m0} between 2.5 - 3m contain more than 80% of swells. Waves from NW are short
167 period waves with H_{m0} between 0.5 and 1.5; in which swell percentage is very less showing the
168 influence of wind-sea generated by sea breeze (Fig. 3d). High waves observed in the study area
169 consists of more than 80% swells.

170

171 Date versus year plots of significant wave height (Fig. 4) shows that H_{m0} has its maximum
172 values ($H_{m0} > 3$ m) during the monsoon period with a wave direction of WSW and peak wave period
173 of 10 - 12s (intermediate period). The mean wave period shows its maximum values (6 - 8s) during
174 the monsoon period. During January–May in all the years, H_{m0} is low ($H_{m0} < 1$ m) with waves from
175 SW, W and NW directions. NW waves observed are the result of strong sea breezes existing during
176 this period. Both long-period ($T_p > 14$ s), intermediate-period ($10 < T_p < 14$ s) and short-period (T_p
177 < 8 s) waves are observed during this period and hence, the mean wave period observed is low
178 compared to monsoon (Fig. 4d). During October to December, similar to the pre-monsoon period,
179 H_{m0} observed is less than 1m, but wave direction is predominantly SW and W, with least NW
180 waves. Short period waves are almost absent during this period and the condition is same for all the
181 years. The interannual variations in H_{m0} are less than 15% (Fig. 4). Primary seasonal variability in



182 waves is due to the monsoonal wind reversal. During January-March, there is a shift in the
183 occurrences of northwest swells.

184

185 Most of the wave conditions ($\sim 75\%$) are to be intermediate and shallow-water waves at the
186 buoy location (where water depth is less than half the wavelength, $d < L/2$), this condition is not
187 satisfied during $\sim 25\%$ of time due to waves with mean periods of 4.4 s or less. This study,
188 therefore, deals with shallow, intermediate and deepwater wave climatology. Hence, bathymetry
189 will significantly influence the wave characteristics.

190

191 4.2 Wave spectrum

192

193 The normalized wave spectral energy density contours are presented for different years to
194 know the wind-sea/swell predominance (Fig. 5). The predominance of both the wind-seas and
195 swells are observed in the non-monsoon period, whereas in the monsoon only swells are
196 predominant (Fig. 5). Over an annual cycle, around 54% of the waves are due to swells. Glejin et
197 al. (2012) reported that the dominance of swells during monsoon is due to the fact that even though
198 the wind at the study region is strong during monsoon, the wind over the entire AS also will be
199 strong and when these swells are added to the wave system at the buoy location, the energy of the
200 swell increases (Donelan, 1987) and will result in dominance of swells. The spread of spectral
201 energy to higher frequencies (0.15 to 0.25 Hz) is predominant during January-May (Fig. 5) due to
202 sea-breeze in the pre-monsoon period (Neetu et al., 2006; Dora and Sanil Kumar, 2015). In the
203 monsoon during the wave growth period, the spectral peak shifted from 0.12-0.13 Hz to 0.07-0.09
204 Hz (lower frequencies).

205

206 An interesting phenomenon is that the long-period (> 18 s) swells are present for 2.5% of
207 the time during the study period. The buoy location at 15 m water depth is exposed to waves from
208 northwest to south with the nearest landmass at ~ 1500 km in the northwest (Asia), ~ 2500 km in
209 the west (Africa), ~ 4000 km in the southwest (Africa) and ~ 9000 km in the south (Antarctica)
210 (Amrutha et al., 2016). Due to its exposure to the Southern Oceans and the large fetch available,
211 swells are present all year round in the study area and the swells are dominant in the non-monsoon
212 (Glejin et al., 2013). Throughout the year, the low-frequency (< 0.1 Hz) waves are the southwest
213 swells whereas with seasons the direction of high-frequency waves changes (Fig. 5). Amrutha et al.
214 (2016) reported that the long-period waves observed in the eastern AS are the swells generated in



215 the south Indian Ocean. In the monsoon season, the waves with high-frequency are predominantly
216 from west-southwest, whereas in the non-monsoon they are from the northwest. In the non-
217 monsoon period, the predominance of wind-seas and swells fluctuated and hence the mean wave
218 direction also changed frequently (Fig. 5).

219

220 The interannual changes of wave spectral energy density for different months in the period
221 2011-2015 are studied by computing the monthly average wave spectra for all the years (Fig. 6).
222 Except during the monsoon period, the wave spectra observed is double-peaked, indicating the
223 presence of wind-seas and swells, whereas during the monsoon, due to the strong southwest winds,
224 single peaked spectrum is observed, i.e. the swell peak with low-frequency and high spectral energy
225 density. Along the Indian coast, Harish and Baba (1986), Rao and Baba (1996) and Sanil Kumar et
226 al. (2003) found out that the spectra are generally multi-peaked and the double peaked wave spectra
227 are more during low-sea states (Sanil Kumar et al., 2004). Sanil Kumar et al. (2014), Sanil Kumar
228 and Anjali (2015) and Anjali and Sanil Kumar (2016) have also observed double-peaked spectrum
229 in the monsoon period in the eastern AS are due to the locally generated wind-seas and the south
230 Indian Ocean swells. From January to May and October to December, the swell peak is between the
231 frequencies 0.07 and 0.08 Hz ($12.5 < T_p < 14.28s$), but in the monsoon period, the swell peak is
232 around 0.1 Hz, in all the years studied. This shows long-period swells ($T_p > 13s$) in the non-
233 monsoon period and intermediate period swells ($8 < T_p < 13s$) in the monsoon. Glejtin et al. (2016),
234 also observed the presence of low-amplitude long-period waves in the eastern AS in the non-
235 monsoon period and intermediate period waves in the monsoon period. This is because of the
236 propagation of swells from the southern hemisphere is more visible during the non-monsoon period
237 due to the calm conditions (low wind-seas) prevailing in the eastern AS. Whereas during the
238 monsoon period, these swells are less due to the turbulence in the north Indian Ocean (Glejtin et al.,
239 2013). Large interannual variations are observed for monthly average wave spectrum in all months
240 except in July. This is because July is known to be the roughest month over the entire annual cycle
241 and southwest monsoon reaches its peak during July. Hence, the influence of temporally varying
242 wind-seas on the wave spectrum is least during July compared to other months. Maximum spectral
243 energy observed is during June 2013 due to the early onset (on 1 June) and advancement of
244 monsoon during 2013 compared to other years. The wave spectra of November 2011 is distinct
245 from that of other years, with low wind-sea peak frequency, i.e. 0.13 Hz due to the deep depression
246 ARB04, occurred south of India near Cape Comorin, during 26 November–1 December, with a



247 sustained wind speed of 55 km/h. During October 2014, the second peak is observed at 0.11 Hz
248 with comparatively high energy showing the influence of cyclonic storm NILOFAR. It is an
249 extremely severe cyclonic storm occurred during the period 25-31 October 2014, originated from a
250 low-pressure area between Indian and Arabian Peninsula, with the highest wind speed of 215 km/h
251 and affected the areas of India, Pakistan and Oman. Significant interannual variation is observed in
252 the wind-sea peak frequency. Wave spectra averaged over each season (Fig. 7) shows that the
253 interannual variations in energy spectra averaged over full year period almost follows the pattern of
254 monsoon spectra, indicating the strong influence of monsoon winds over the wave energy spectra in
255 the study area. Interannual variations within the spectrum are more for wind-seas compared to
256 swells. During the study period, the maximum spectral energy observed is during 2011 monsoon.

257

258 For different frequencies, the monthly average wave direction are shown in Fig. 8. It is
259 observed that throughout the year the mean wave direction of the swell peak is southwest (200-
260 250°). In the non-monsoon period, the wind-sea direction is northwest (280-300°), except in
261 October and November. This is due to the wind-seas produced by sea breeze which has the
262 maximum intensity during the pre-monsoon season. Interannual variability in wave direction is
263 more during October and November, where the wind-seas from southwest direction are also
264 observed. This is because, during these months, the wind speed and the strength of the monsoon
265 swell decreases, which makes the low energy wind-seas produced by the withdrawing monsoon
266 winds more visible.

267

268 Contour plots of spectral energy density (normalized) clearly show the predominance of
269 wind-seas and swells during the non-monsoon period (Fig. 9). In the monsoon period, the spectral
270 energy density is mainly confined to a narrow frequency range (0.07-0.14 Hz) and the wave spectra
271 are mainly single peaked. Glejin et al. (2012) reported that in the monsoon season, the spectral peak
272 is between 0.08 and 0.1 Hz (12-10s) for ~ 72% of the time in the eastern AS. Earlier studies also
273 reported dominance of swells in the eastern AS during the monsoon (Sanil Kumar et al., 2012;
274 Glejin et al., 2012). Wind-sea energy is comparatively low during October, November and
275 December and occurs mostly in the frequency range less than 0.2 Hz, whereas, during January-
276 May, the frequency exceeds 0.2 Hz. In the pre-monsoon period, wind-sea plays a major role in
277 nearshore wave environment (Rao and Baba, 1996). Wind-sea energy is found to be low during



278 April 2015 (Fig. 6), because of reduction in local winds. The occurrence of wind-seas is very less
279 during most of the time in November except during 2011, due to the deep depression ARB04.

280

281 To study the characteristics of different wave systems, average mean wave direction and
282 average wave spectral energy density grouped under different peak frequency bins are plotted in
283 Fig. 10. Wave spectrum is mostly single peaked at low-frequency bins and multi-peaked at higher
284 frequencies. Within the frequency range 0.07 to 0.15 Hz, the spectrum observed is a smooth single
285 peaked spectrum, with high energy density. Maximum energy observed is within the frequency
286 range 0.08-0.1 Hz, having direction 240° which indicates the monsoon swells. Above 0.15 Hz, even
287 though the spectrum is multi-peaked, energy gradually decreases, with the lowest energy observed
288 between 0.3 and 0.5 Hz. Between 0.15 and 0.5 Hz, waves observed are from the northwest
289 direction (300°) and represents the wind-seas produced by local winds. Long period swells ($T_p >$
290 14s) are also observed from the southwest. The average direction of waves with $H_{m0} < 1\text{m}$ shows
291 the northwest wind-seas and the southwest swells, whereas for high waves ($H_{m0} > 3\text{m}$), the
292 difference between the swell and wind-sea direction decreases (Fig. 11). This is because the high
293 waves get aligned to the bottom contour before 15 m water depth on its approach to the shallow
294 water.

295

296 The behavior of the high-frequency part of the spectrum is governed by the energy balance
297 of waves generated by the local wind fields. When the wind blows over a long fetch or for a long
298 time, the wave energy for a given frequency reaches the equilibrium range and the energy input
299 from the wind are balanced by energy loss to other frequencies and by wave breaking
300 (Torsethaugen and Haver, 2004). The high-frequency tail slope of the monthly average wave
301 spectrum in different years (Table 4) shows that the slope is high (> 3.1), during June to September
302 and the case is same for all the years studied. During all other months, the slope is within the range
303 1.5 - 3.1. The distribution of slope values for different significant wave height ranges shows that the
304 slope increases from 2.44 to 4.2 as the significant wave height increases and reaches a saturation
305 range. For frequencies from 0.229 to 0.58 Hz in the eastern AS during January-May, Amrutha et al.
306 (2016) observed that the high-frequency tail has $f^{2.5}$ pattern at 15 m water depth and for
307 frequencies ranging from 0.315 to 0.55 Hz, the high-frequency tail follows f^3 at 5 m water depth. It
308 is shown in Fig. 12 that the slope also increases as the mean wave period increases. Since H_{m0} is
309 maximum during the monsoon period, the slope is also maximum during June to September. There



310 is no much interannual variation in slope for swell dominated spectra during the monsoon, while in
311 the non-monsoon period when wind-seas have much influence, the slope varies significantly. The
312 slope of the high-frequency end of the wave spectrum becomes milder when the wave nonlinearity
313 increases. The study shows that the tail of the spectrum is influenced by the local wind conditions.

314

315 4.3 Theoretical wave spectra

316

317 The monthly average wave spectra for the year 2015, is compared with JONSWAP and
318 Donelan theoretical wave spectra. It is found that JONSWAP and Donelan spectra with modified
319 parameters describe well the wave spectra at low frequencies and high frequencies respectively.
320 From Fig. 13, we can see that spectrum is double peaked during January-April and December. For
321 these months the first peak is fitted with JONSWAP spectrum and second with Donelan, and the
322 fitted spectrum shows a good match with the measured one. In the monsoon period, the spectrum is
323 single peaked with high spectral energy density and during this period JONSWAP spectrum is
324 fitted up to the peak frequency and after that Donelan spectrum is used. During the months May,
325 October and November, after the peak frequency, the measured spectrum is not smooth and hence
326 for this part, Donelan spectrum is fitted in two parts in order to obtain the best fit. Here also
327 JONSWAP shows best fit, up to the peak frequency.

328

329 The values for α and Υ were randomly varied within a range to find out the values for
330 which, the theoretical spectrum best fits the measured spectrum and those values were used to plot
331 the theoretical spectrum. The values of α and Υ thus obtained, for each month and the range of
332 frequencies for which each spectrum is plotted are given in Table 6. From the table, the average
333 values of α and Υ , over 1-year period are obtained as 0.0050 and 1.33 for JONSWAP spectra and
334 0.0254 and 1.27 for Donelan spectra respectively. These values are less than the generally
335 recommended values of α and Υ ; 0.0081 and 3.3. α is a constant that is related to the wind speed
336 and fetch length. From the table, it can be seen that α has the highest values during the months June
337 to August and is the same for both JONSWAP and Donelan spectrum. This may be due to the high
338 wind speed during monsoon. High values of α were also observed during November, February and
339 April, since these are the months during which sea breeze has maximum influence, high α values is
340 due to the influence of local winds. There is no seasonal variation observed in the values of Υ . For
341 all the months, Donelan spectrum fitted is proportional to f^4 , except during May and November,



342 where spectrum is proportional to $f^{2.8}$ and $f^{2.5}$, above frequencies 0.15 Hz and 0.28 Hz
343 respectively. The theoretical spectrum JONSWAP and Donelan cannot completely describe the
344 high-frequency tail of the measured spectrum since the high-frequency tail in these spectrum
345 decays in the form of f^5 and f^4 respectively. Since the high-frequency slope of the wave spectrum
346 is within the range 3-4 during the monsoon period, Donelan spectrum shows better fit for monsoon
347 spectra compared to other months (Fig. 13).

348

349 5. Concluding remarks

350

351 In this paper, the variations in the wave spectral shapes in different months for a nearshore
352 location are investigated based on in situ wave data obtained from moored directional waverider
353 buoy. Interannual variations within the spectrum are more for wind-seas compared to swells. The
354 maximum significant wave height measured at 15 m water depth is 5 m and the annual average H_{m0}
355 has similar value (~1.1 m) in all the years. Over the 5 years, small waves ($H_{m0} < 1$ m) account for a
356 large proportion of measured data (63.94% of the time). The study shows that high waves ($H_{m0} > 2$
357 m) are with spectral peak period between 8 and 14 s and the long period swells (14-20 s) are with
358 $H_{m0} < 2.5$ m. The high-frequency slope of the wave spectrum varies from 2.44 to 4.2 and it
359 increases with increase in significant wave height and mean wave period. During the monsoon
360 period, Donelan spectrum shows better fit for monsoon spectra compared to other months since the
361 high-frequency slope of the wave spectrum is within the range 3-4. The decay of the high-
362 frequency waves are fastest with depth and hence, the high-frequency tail values observed in the
363 study will be different for different water depths.

364

365 Acknowledgments

366 The authors acknowledge the Earth System Science Organization, Ministry of Earth
367 Sciences, New Delhi for providing the financial support to conduct part of this research. We thank
368 TM Balakrishnan Nair, Head OSISG and Arun Nherakkol, Scientist, INCOIS, Hyderabad and Jai
369 Singh, Technical Assistant, CSIR-NIO for the help during the collection of data. We thank Dr. Bhat
370 and Dr. J L Rathod, Department of Marine Biology, Karnataka University PG Centre, Karwar for
371 providing the logistics required for wave data collection. This work contributes part of the Ph.D.
372 work of the first author. This paper is dedicated to the memory of our esteemed colleague Ashok



373 Kumar, in recognition of his substantial contributions in initiating the wave measurements in the
374 shallow waters around India. This publication is a NIO contribution.

375

376 **References**

377

378 Amrutha, M.M., Sanil Kumar, V., and George, J.: Characteristics of inter-monsoon long-period
379 waves in the nearshore waters of central west coast of India, *Ocean Engineering* (in review), 2016.

380 Anjali, N.M., and Sanil Kumar, V.: Spectral wave climatology off Ratnagiri - northeast Arabian
381 Sea, *Natural Hazards*, 82, 1565-1588, 2016.

382 Ardhuin, F., Chapron, B., and Collard, F.: Observation of swell dissipation across oceans, *J.*
383 *Geophys. Res.-Oceans.*, 36, 1–5, 2009.

384 Carter, R.W.G.: Coastal environments: an introduction to the physical, ecological and cultural
385 systems of coastlines, in: Academic Press., London, 1988.

386 Cavaleri, L., Fox-Kemper, B., and Hemer, M.: Wind-waves in the coupled climate sys- tem. *Bull.*
387 *Am. Meteorol. Soc.*, 93, 1651–1661, 2012.

388 Chakrabarti, S.K.: Handbook of Offshore Engineering, Vol-1, Ocean Engineering Series, Elsevier,
389 p 661, 2005.

390 Chen, G., Chapron, B., Ezraty, R., and Vandemark, D.: A global view of swell and wind-sea
391 climate in the ocean by satellite altimeter and scatterometer. *J. Atmospheric and Oceanic*
392 *Technology.*, 19(11), 1849-1859, 2002.

393 Chen, Q., Zhao, H., Hu, K., and Douglass, S.L.: Prediction of Wind Waves in a Shallow Estuary, *J.*
394 *Waterway, Port, Coastal, and Ocean Eng.*, 131 (4), 137-148, 2005.

395 Dattatri, J.: Coastal Erosion and Protection along Karnataka Coast, Centre for Environmental Law,
396 Education, Research and Advocacy (CEERA), The National Law School of India University, 2007.

397 Donelan, M. A.: The effect of swell on the growth of wind waves, *Johns Hopkins APL Technical*
398 *Digest.*, 8 (1), 18-23, 1987.



- 399 Donelan, M., Hamilton, H., and Hui, W.H.: Directional spectra of wind-generated waves,
400 Philosophical Transactions of the Royal Society of London A: Mathematical, Physical and
401 Engineering Sciences., 315(1534), 509-562, 1985.
- 402 Dora, G.U., and Sanil Kumar, V.: Sea state observation in island-sheltered nearshore zone based on
403 in situ intermediate-water wave measurements and NCEP/CFSR wind data, Ocean Dynamics., 65,
404 647-663, 2015.
- 405 Drennan, W. M., Kahma, K.K., and Donelan, M.A.: On momentum flux and velocity spectra over
406 waves, Boundary-Layer Meteorology., 92(3), 489-515, 1999.
- 407 Glejin, J., Sanil Kumar, V., Balakrishnan Nair, T. M., and Singh, J.: Influence of winds on
408 temporally varying short and long period gravity waves in the near shore regions of the eastern
409 Arabian Sea, Ocean Sci., 9, 343–353, doi:10.5194/os-9-343-2013, 2013.
- 410 Glejin, J., Sanil Kumar, V., Sajiv, P.C., Singh, J., Pednekar, P., Ashok Kumar, K., Dora, G.U., and
411 Gowthaman, R.: Variations in swells along eastern Arabian Sea during the summer monsoon, Open
412 J. Mar. Sci., 2 (2), 43–50, 2012.
- 413 Glejin, J., Sanil Kumar, V., Amrutha, M.M. and Singh J.: Characteristics of long-period swells
414 measured in the in the near shore regions of eastern Arabian Sea, Int. J. Naval Architecture and
415 Ocean Engineering, 8, 312-319, 2016.
- 416 Goda, Y.: A review on statistical interpretation of wave data, Report of the Port and Harbour
417 Research Institute, Japan 18, 5–32, 1979.
- 418 Goda, Y.: On the methodology of selecting design wave height, Proceedings 21st International
419 Conference Coastal Engineering, Malaga, 899-913, 1988.
- 420 Gringorten, I.I.: A plotting rule for extreme probability paper, J. Geophysical Res., 68 (3), 813-814,
421 1963.
- 422 Guedes Soares, C., Cherneva, Z., and Antao, E.M.: Steepness and asymmetry of the largest waves
423 in storm sea states, Ocean Eng., 31(8), 1147-1167, 2004.
- 424 Gumbel, E.J.: Statistics of Extremes, Columbia University Press, New York, USA, 1958.



- 425 Gunson, J., and Symonds, G.: Spectral Evolution of Nearshore Wave Energy during a Sea-Breeze
426 Cycle, *J. Phys. Oceanogr.*, 44(12), 3195-3208, 2014.
- 427 Hanamgond, P.T., and Mitra, D.: Dynamics of the Karwar Coast, India, with special reference to
428 study of Tectonics and Coastal Evolution using Remote Sensing Data, *J. Coastal Research.*, Special
429 Issue 50, 842-847, 2007.
- 430 Hanley, K. E., Belcher, S.E., and Sullivan, P.P.: A global climatology of wind–wave interaction, *J.*
431 *Phys. Oceanogr.*, 40(6), 1263-1282, 2010.
- 432 Hanson, J.L., and Phillips, O.M.: Wind-sea growth and dissipation in the open ocean, *J. Phys.*
433 *Oceanogr.*, 29, 1633-1648, 1999.
- 434 Harish, C. M., and Baba, M.: On spectral and statistical characteristics of shallow water waves,
435 *Ocean Eng.*, 13(3), 239-248, 1986.
- 436 Hasselmann, K., Barnett, T.P., Bouws, F., Carlson, H., Cartwright, D.E., Enke, K., Ewing J.A.,
437 Gienapp, H., Hasselmann, D.E., Krusemann, P., Meerburg, A., Muller, P., Olbers, D.J., Richter, K.,
438 Sell, W., and Walden, H.: Measurements of wind-wave growth and swell decay during the Joint
439 North Sea Wave Project (JONSWAP), *Deutsches Hydrographisches Institut.*, A8 (12), 95, 1973.
- 440 Hasselmann, K., Ross, D.B., Miller, P., and Sell, W.: A parametric wave prediction model, *J. Phys.*
441 *Oceanogr.*, 6, 200-228, 1976.
- 442 Houlthuijsen, L. H.: *Waves in oceanic and coastal waters*, Cambridge University Press, 2007.
- 443 Hwang, P.A., Garcia-Nava, H., and Ocampo-Torres, F.J.: Dimensionally Consistent Similarity
444 Relation of Ocean Surface Friction Coefficient in Mixed Seas, *J. Phys. Oceanogr.* 41., 1227–1238.
445 2011.
- 446 Kuik, A. J., Vledder, G., and Holthuijsen, L.H.: A method for the routine analysis of pitch and roll
447 buoy wave data, *J. Phys. Oceanogr.*, 18, 1020–1034, 1988.
- 448 Longuet-Higgins, M.S.: On the joint distribution of the periods and amplitudes of sea waves, *J.*
449 *Geophys. Res.-Oceans.*, 80, 2688–2694, 1975.



- 450 Neetu, S., Shetye Satish., and Chandramohan, P.: Impact of sea breeze on wind-seas off Goa, west
451 coast of India, *Journal Earth System Science.*, 115, 229-234, 2006.
- 452 Nigam, R., and Khare, N.: Significance of correspondence between river discharge and proloculus
453 size of benthic Foraminifera in paleomonsoonal studies, *Geo-Marine Letters.*, 15 (1), 45-50, 1995.
- 454 Pierson, W.J., and Moskowitz, L.: A proposed form for fully developed seas based on the similarity
455 theory of S.A.Kitaigorodski, *J. Geophys. Res.-Oceans.*, 69(24), 5181-5190, 1964.
- 456 Portilla, J., Ocampo-Torres, F.J., and Monbaliu, J.: Spectral Partitioning and Identification of
457 Wind-sea and Swell, *J. Atmospheric and Oceanic Technology.*, 26, 117-122, 2009.
- 458 Rao, C. P., and Baba, M.: Observed wave characteristics during growth and decay: a case study,
459 *Continental Shelf Res.*, 16(12), 1509-1520, 1996.
- 460 Sanil Kumar, V., Johnson, G., Dora, G.U., Chempalayil, S.P., Singh, J., and Pednekar, P.:
461 Variations in nearshore waves along Karnataka, west coast of India, *J. Earth Systems Science.*, 121,
462 393-403, 2012.
- 463 Sanil Kumar, V., Anand, N.M., Kumar, K.A., and Mandal, S.: Multipeakedness and groupiness of
464 shallow water waves along Indian coast, *J. Coastal Res.*, 19, 1052-1065, 2003.
- 465 Sanil Kumar, V., and Anand, N.M.: Variation in wave direction estimated using first and second
466 order Fourier coefficients, *Ocean Eng.*, 31, 2105–2119, 2004.
- 467 Sanil Kumar, V. and Anjali Nair, M.: Inter-annual variations in wave spectral characteristics at a
468 location off the central west coast of India, *Ann. Geophys.*, 33, 159–167, doi:10.5194/angeo-33-
469 159-2015, 2015.
- 470 Sanil Kumar, V., and Kumar, K.A.: Spectral representation of high shallow water waves, *Ocean*
471 *Eng.*, 35, 900-911, 2008.
- 472 Sanil Kumar, V., Shanas, P.R., and Dubhashi, K.K.: Shallow water wave spectral characteristics
473 along the eastern Arabian Sea, *Natural Hazards*, 70, 377–394, 2014.
- 474 Semedo, A., Sušelj, K., Rutgeresson, A., and Sterl, A.: A global view on the wind-sea and swell
475 climate and variability from ERA-40, *J. Climate*, 24(5), 1461-1479, 2011.



- 476 Shetye, S.R., Shenoi, S.S.C., Antony, A.K., and Kumar, V.K.: Monthly-mean wind stress along the
477 coast of the north Indian Ocean, *J. Earth Syst. Sci.*, 94, 129–137, doi:10.1007/BF02871945, 1985.
- 478 Shore Protection Manual, U.S. Army Coastal Engineering Research Center, Department of the
479 Army, Corps of Engineers, U.S. Govt. Printing Office, Washington, DC, USA, vols. 1 and 2, 1984.
- 480 Stephen, F.B., and Tor Kollstad.: Field trials of the directional waverider, *Proceedings of the First*
481 *International Offshore and Polar Engineering Conference*, Edinburgh, III 55–63, 1991.
- 482 Torsethaugen, K., and Haver, S.: Simplified double peak spectral model for ocean waves, In:
483 *Proceeding of the 14th International Offshore and Polar Engineering Conference*, 2004.
- 484 Yuan, Y., and Huang, N.E.: A reappraisal of ocean wave studies, *J. Geophys. Res.-Oceans.*,
485 117(C11), 2012.
- 486



487 **Figure captions**

488 Figure 1. Study area along with the wave measurement location in eastern Arabian Sea

489 Figure 2. Time series plot of a) significant wave height, b) mean wave period, c) peak wave period
490 and d) mean wave direction from 1 January 2011 to 31 December 2015. Thick blue line indicates
491 the monthly average values

492 Figure 3. Wave roses during 2011-2015 (a) significant wave height and mean wave direction, (b)
493 peak wave period and mean wave direction, (c) percentage of swell, (d) percentage of wind-sea and
494 mean wave direction

495 Figure 4. Date versus year plot of a) significant wave height b) mean wave direction, c) peak wave
496 period and d) mean wave period

497 Figure 5. Temporal variation of normalized spectral energy density (top panel) and mean wave
498 direction (bottom panel) with frequency in different years

499 Figure 6. Monthly average wave spectra in 2011 to 2015

500 Figure 7. Wave spectra averaged over a) pre-monsoon (February-May), b) monsoon (June-
501 September), c) post-monsoon (October-January) and d) full year in different years

502 Figure 8. Monthly average wave direction at different frequencies in different months

503 Figure 9. Temporal variation of normalized spectral energy density in different months (data from
504 2011 to 2015 used)

505 Figure 10. Plot of average spectral energy density and average mean wave direction of waves
506 grouped under different peak frequency bins

507 Figure 11. Plot of a) average spectral energy density and b) average mean wave direction of waves
508 under different H_{m0} with frequency

509 Figure 12. Plot of high frequency tail with significant wave height (left panel) and with mean wave
510 period (right panel)

511 Figure 13. Fitted theoretical spectra along with the monthly average wave spectra for different
512 month

513



514 Table 1. Number of data used in the study in different years along with range of significant wave
515 height and average value

516

Year	Significant wave height (m)		Number of data	%of data
	Range	Average		
2011	0.3-4.4	1.1	17517	99.98
2012	0.3-3.7	1.1	17323	98.61
2013	0.3-3.6	0.9*	14531	82.94
2014	0.3-4.5	1.1	17284	98.65
2015	0.3-5.0	1.1	14772	84.32

517 * average value is estimated excluding the August month data

518

519

520

521

522

523

524 Table 2. Characteristics of waves in different range of significant wave height

525

Significant wave height range	Number (percentage)	Range of T_p (s)	Mean T_p (s)	Range of T_{m02} (s)	Mean T_{m02} (s)
$H_{m0} < 1$ m	52062 (63.94)	2.6-22.2	12.2	2.7-10.5	4.9
$1 \leq H_{m0} < 2$ m	18297 (22.47)	3.6-22.2	10.5	3.4-10.7	5.7
$2 \leq H_{m0} < 3$ m	9839 (12.08)	6.2-18.0	10.8	5.0-8.9	6.5
$3 \leq H_{m0} < 4$ m	1096 (1.35)	10.0-14.3	11.8	6.1-9.1	7.2
$4 \text{ m} \leq H_{m0}$	133 (0.16)	10.5-14.3	12.6	7.2-9.3	7.8

526

527

528

529

530

531

532 Table 3. Average wave parameters and number of data in different spectral peak frequencies

533

Frequency (f_p) range (Hz)	Number of data and %	H_{m0} (m)	T_{m02} (s)	Peak wave period (s)
$0.04 < f_p \leq 0.05$	318 (0.39)	0.73	5.24	20.19
$0.05 < f_p \leq 0.06$	5341 (6.56)	0.82	5.48	17.16
$0.06 < f_p \leq 0.07$	14764 (18.13)	0.75	5.22	14.73
$0.07 < f_p \leq 0.08$	18221 (22.38)	0.80	5.05	12.96
$0.08 < f_p \leq 0.10$	25364 (31.15)	1.55	5.76	10.88
$0.10 < f_p \leq 0.15$	9459 (11.62)	1.25	5.35	8.07
$0.15 < f_p \leq 0.20$	6355 (7.80)	0.76	4.43	5.72
$0.20 < f_p \leq 0.30$	1487 (1.83)	0.78	3.86	4.36
$0.30 < f_p \leq 0.50$	118 (0.14)	0.66	3.22	3.09

534



535
536
537

Table 4. Slope of the high frequency tail of the monthly average wave spectra in different years

Months	High frequency tail					
	2011	2012	2013	2014	2015	2011-2015
January	-2.08	-2.93	-2.97	-2.72	-2.81	-2.72
February	-2.41	-3.02	-2.74	-2.99	-3.06	-2.85
March	-2.75	-2.91	-2.82	-2.76	No data	-2.81
April	-2.56	-2.74	-2.64	-2.71	-2.19	-2.60
May	-2.59	-2.67	-2.63	-2.42	-2.51	-2.56
June	-3.64	-3.53	-3.55	-3.82	-3.58	-3.55
July	-3.76	-3.55	-3.40	-3.82	-3.63	-3.70
August	-3.63	-3.58	No data	-3.52	-3.65	-3.58
September	-3.41	-3.44	-3.16	-3.38	-3.00	-3.30
October	-2.02	-2.77	-3.03	-2.52	-2.61	-2.68
November	-1.78	-2.43	-1.77	-1.55	-1.65	-1.84
December	-1.69	-2.23	-1.95	-2.06	-1.79	-1.94

538
539
540
541
542
543
544
545
546

Table 5. High frequency tail of the average wave spectra in different wave height ranges

Range of H_{m0} (m)	High frequency tail parameter
0-1	-2.44
1-2	-3.26
2-3	-3.67
3-4	-4.21
4-5	-4.21

547
548

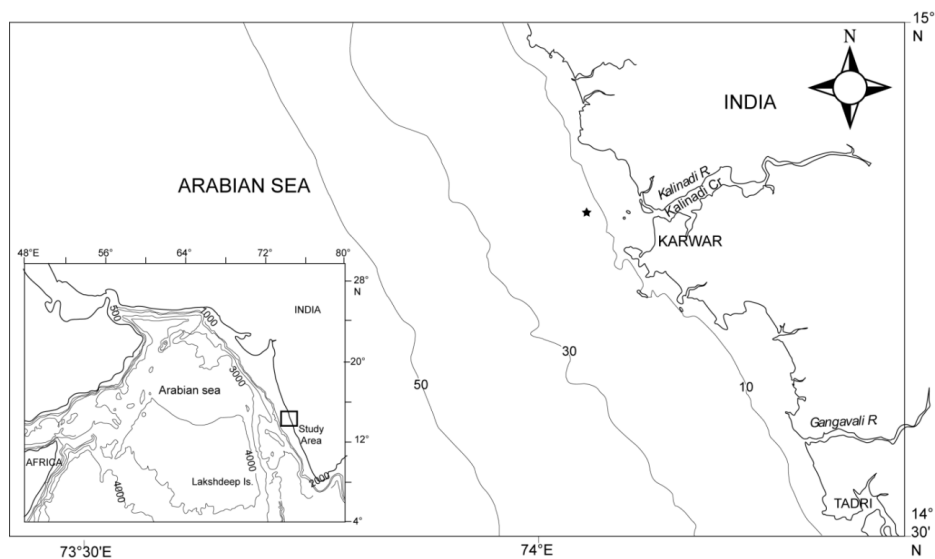


549 Table 6. Parameters of the fitted wave spectrum in different months

Month	Frequency range	JONSWAP spectrum		Frequency range	f ^x (x)	Donelan spectrum	
		α	γ			α	γ
January	0.025-0.095	1.5×10^{-5}	1.6	0.095-0.580	-4	9.8×10^{-4}	1.18
February	0.025-0.090	2.0×10^{-5}	1.4	0.095-0.580	-4	0.0010	1.06
March	0.025-0.095	2.5×10^{-5}	1.2	0.100-0.580	-4	8.7×10^{-4}	1.17
April	0.025-0.100	3.7×10^{-5}	1.4	0.110-0.580	-4	0.0011	1.06
May	0.025-0.070	6.7×10^{-5}	1.1	0.075-0.080	-4	3×10^{-5}	1.92
				0.085-0.090	-4	6×10^{-5}	1.3
				0.095-0.140	-4	1.2×10^{-4}	1.09
				0.150-0.580	-2.8	0.0055	1.09
June	0.025-0.120	0.0014	1.3	0.130-0.580	-4	0.0021	1.33
July	0.025-0.120	0.0012	1.5	0.130-0.580	-4	0.0025	1.23
August	0.025-0.100	0.0014	1.2	0.110-0.580	-4	0.0012	1.4
September	0.025-0.950	7.17×10^{-4}	1.1	0.100-0.580	-4	6.0×10^{-4}	1.02
October	0.025-0.065	4.1×10^{-5}	1.2	0.070-0.095	-4	3×10^{-5}	1.27
				0.100-0.120	-4	8×10^{-5}	1.19
				0.130-0.180	-4	3.9×10^{-4}	1.17
				0.190-0.580	-4	8.9×10^{-4}	1.36
November	0.025-0.070	3.0×10^{-5}	1.4	0.075-0.100	-4	2×10^{-5}	1.6
				0.110-0.140	-4	0.0012	1.43
				0.150-0.270	-4	2.8×10^{-4}	0.74
				0.280-0.019	-2.5	0.0060	1.7
December	0.025-0.095	1.7×10^{-5}	1.6	0.100-0.580	-4	4.9×10^{-4}	1.38

550

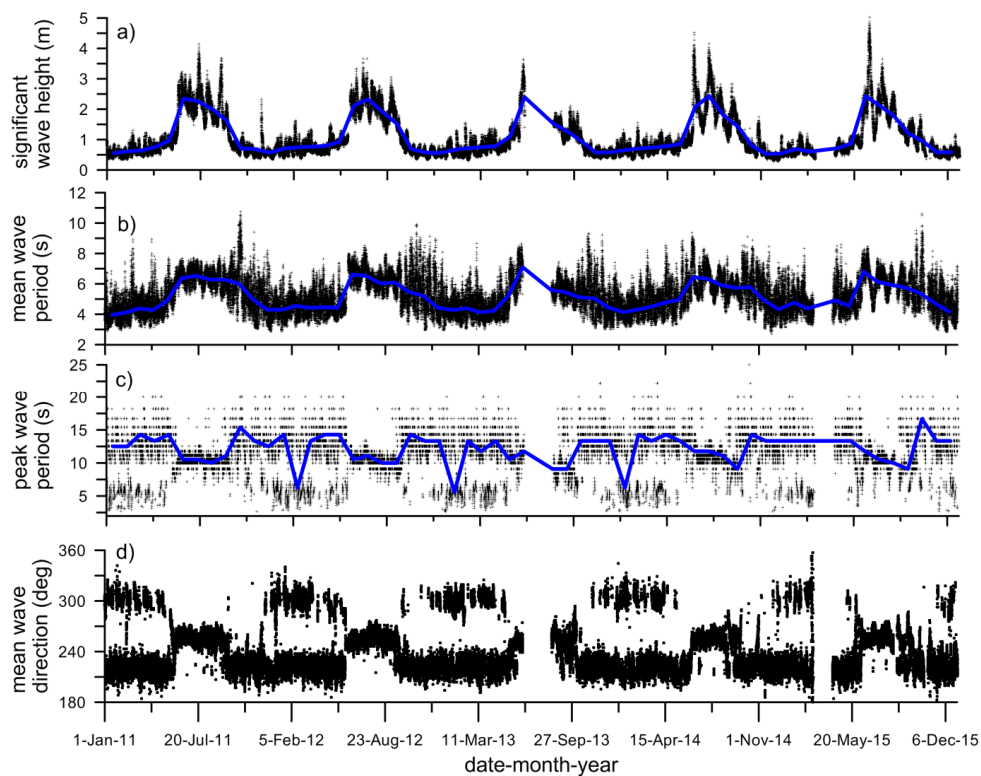
551



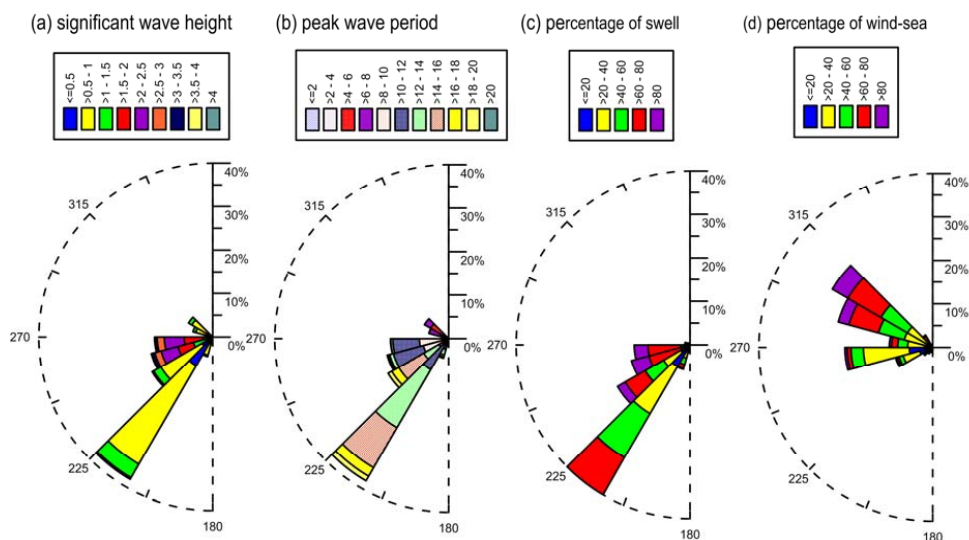
552
553 Figure 1. Study area along with the wave measurement location in eastern Arabian Sea
554



555
556



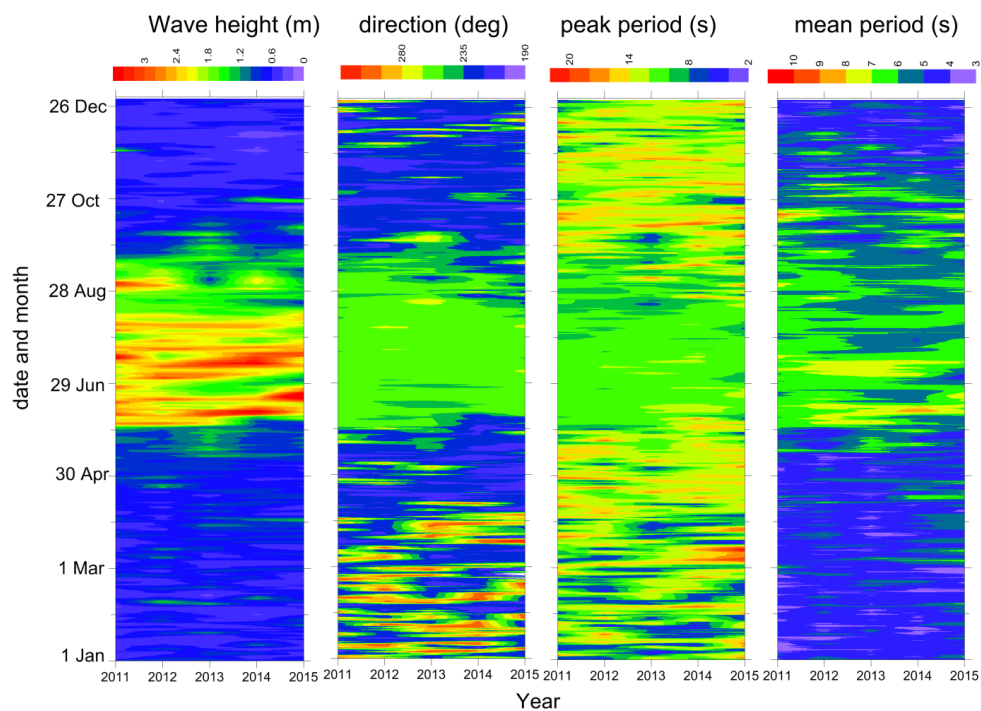
557
558 Figure 2. Time series plot of a) significant wave height, b) mean wave period, c) peak wave period
559 and d) mean wave direction from 1 January 2011 to 31 December 2015. Thick blue line indicates
560 the monthly average values



561
 562 Figure 3. Wave roses during 2011-2015 (a) significant wave height and mean wave direction, (b)
 563 peak wave period and mean wave direction, (c) percentage of swell, (d) percentage of wind-sea and
 564 mean wave direction
 565



566
567

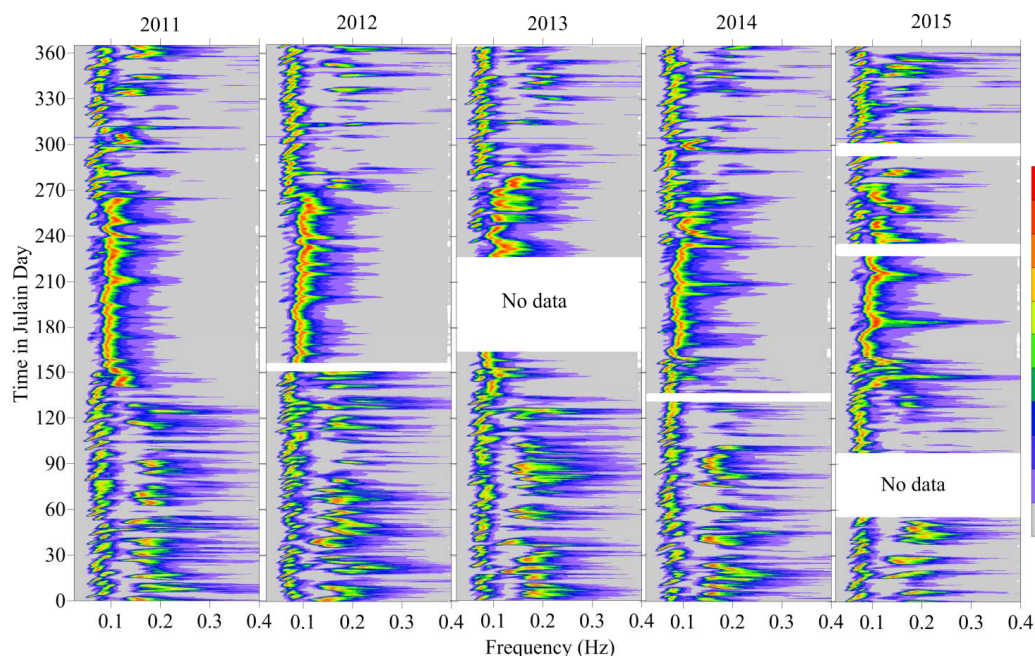


568
569
570
571

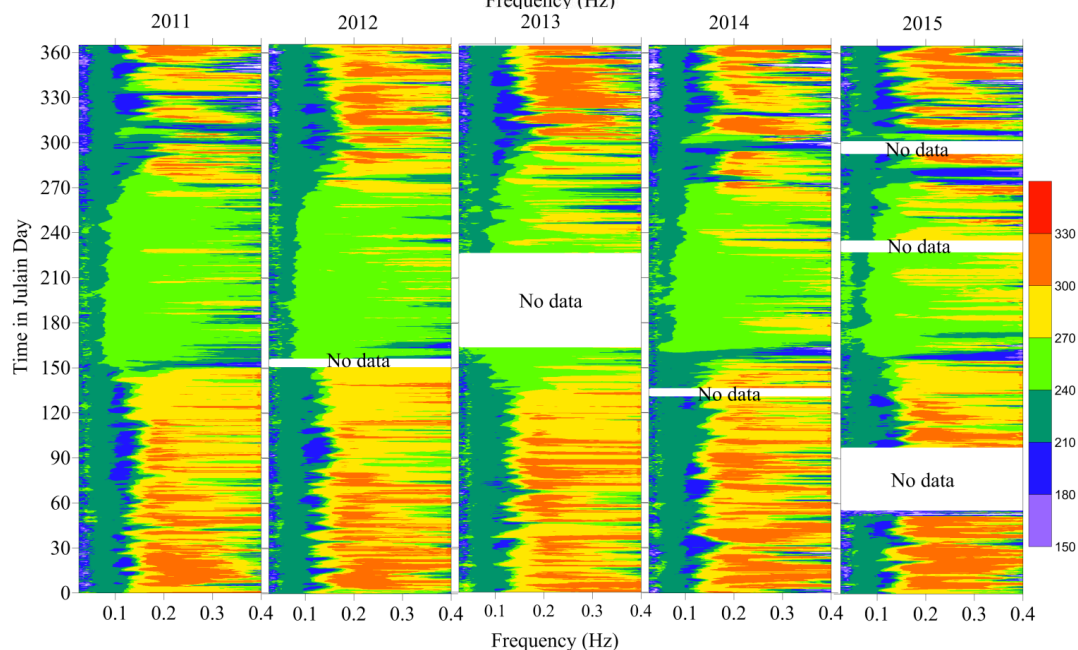
Figure 4. Date versus year plots of a) significant wave height b) mean wave direction, c) peak wave period and d) mean wave period.



572
573

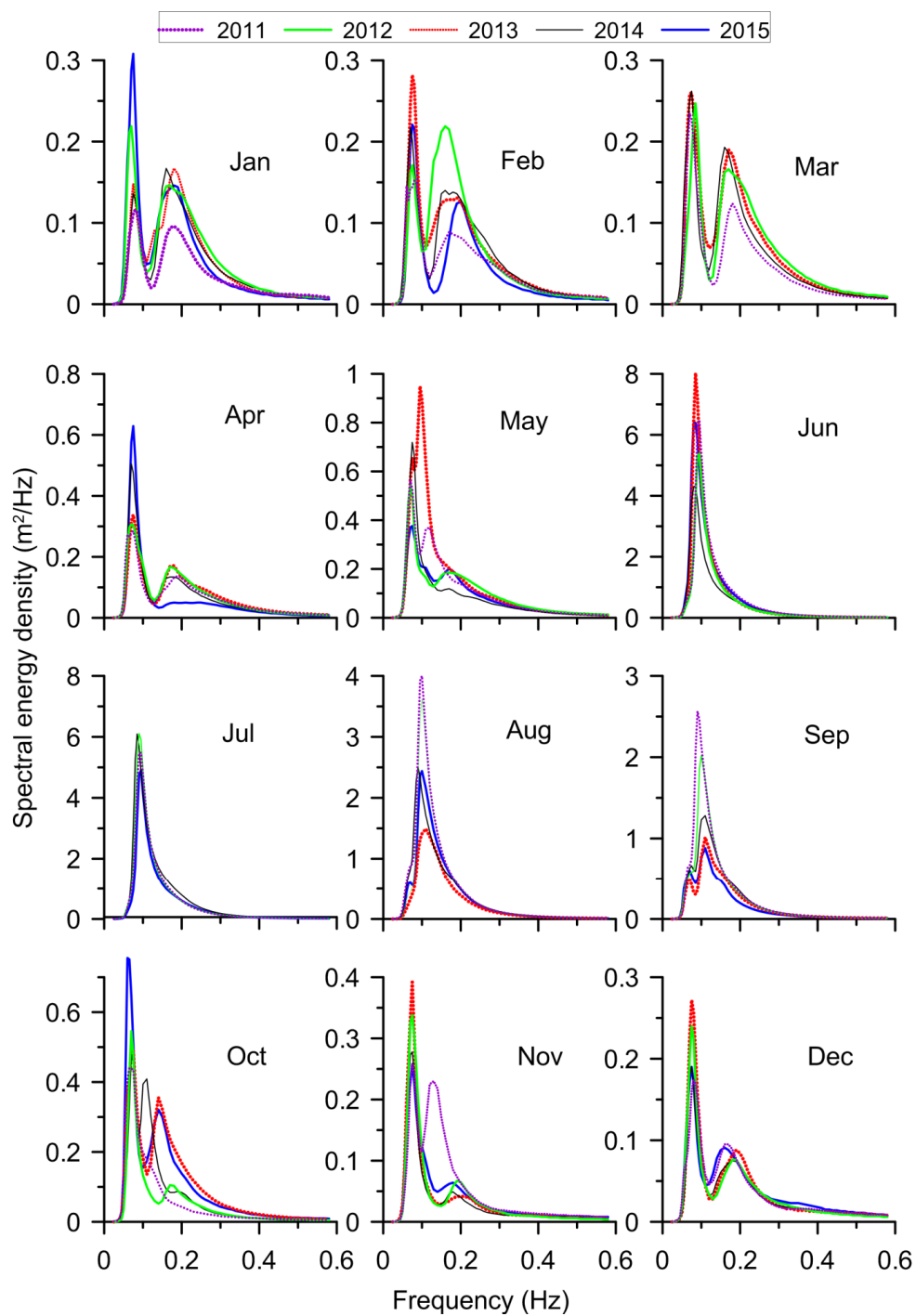


574



575
576
577

Figure 5. Temporal variation of normalized spectral density (top panel) and mean wave direction (bottom panel) with frequency in different years

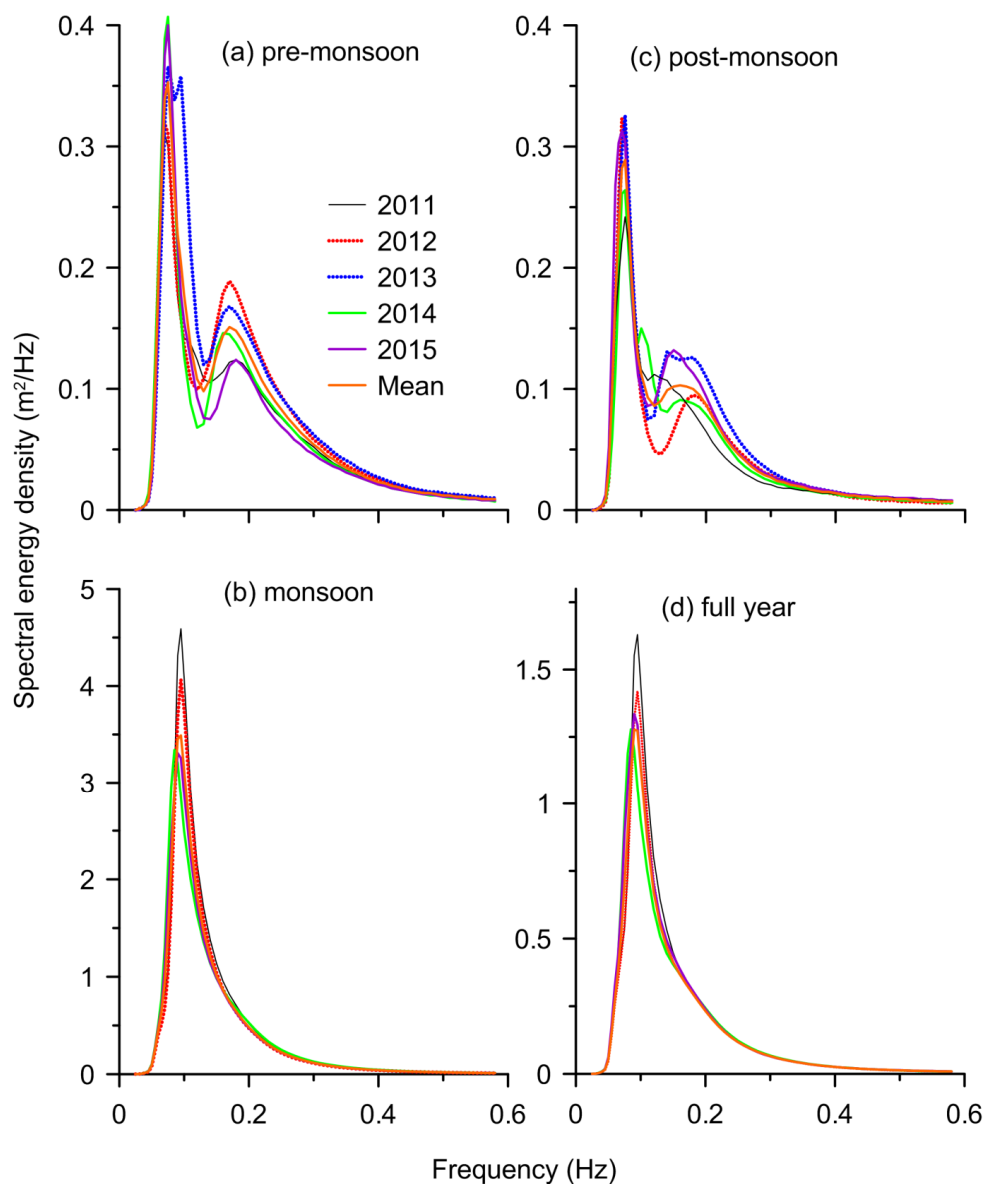


578
579

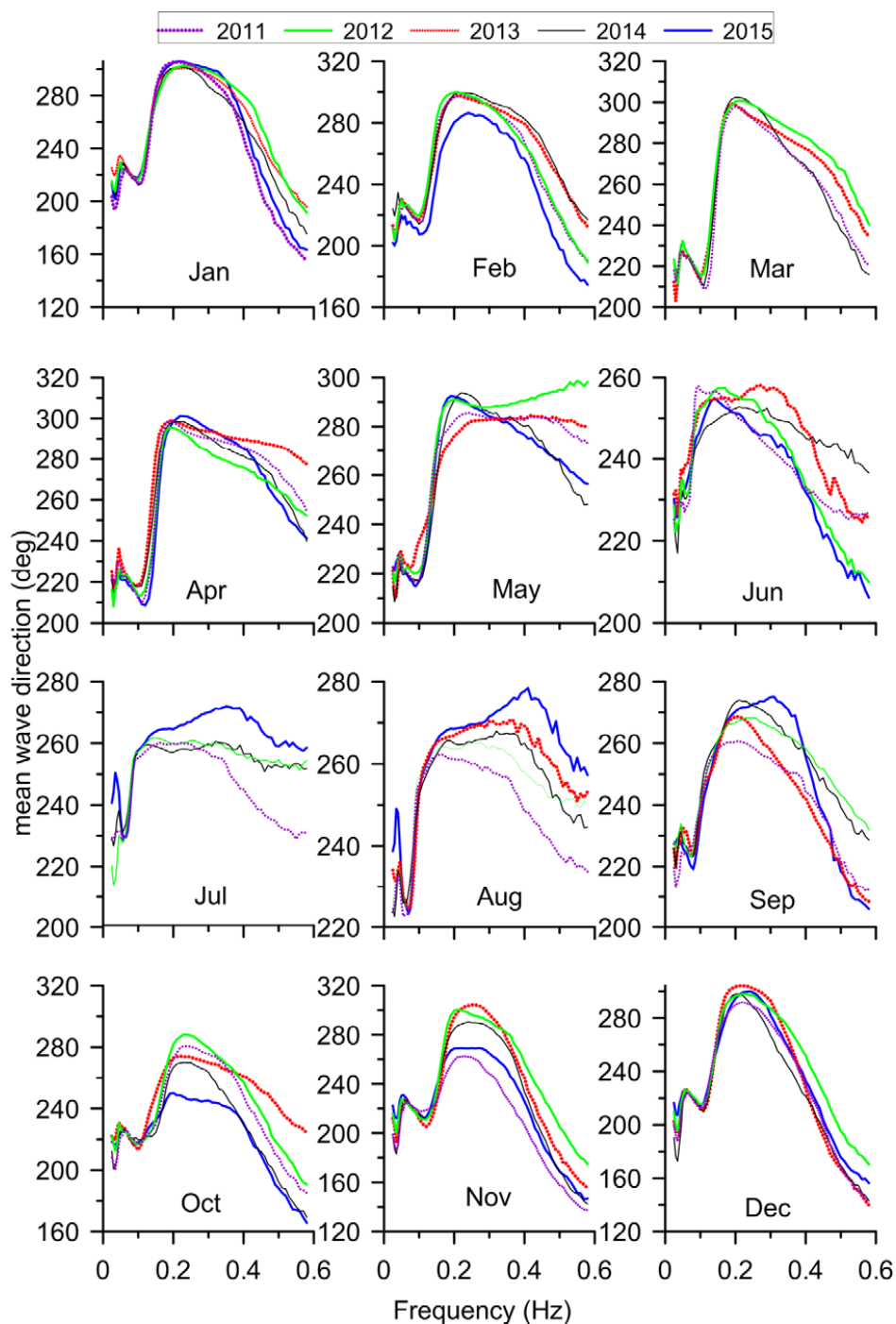
Figure 6. Monthly average wave spectra in 2011 to 2015



580



581
582 Figure 7. Wave spectra averaged over a) pre-monsoon (February-May), b) monsoon (June-
583 September), c) post-monsoon (October-January) and d) full year in different years

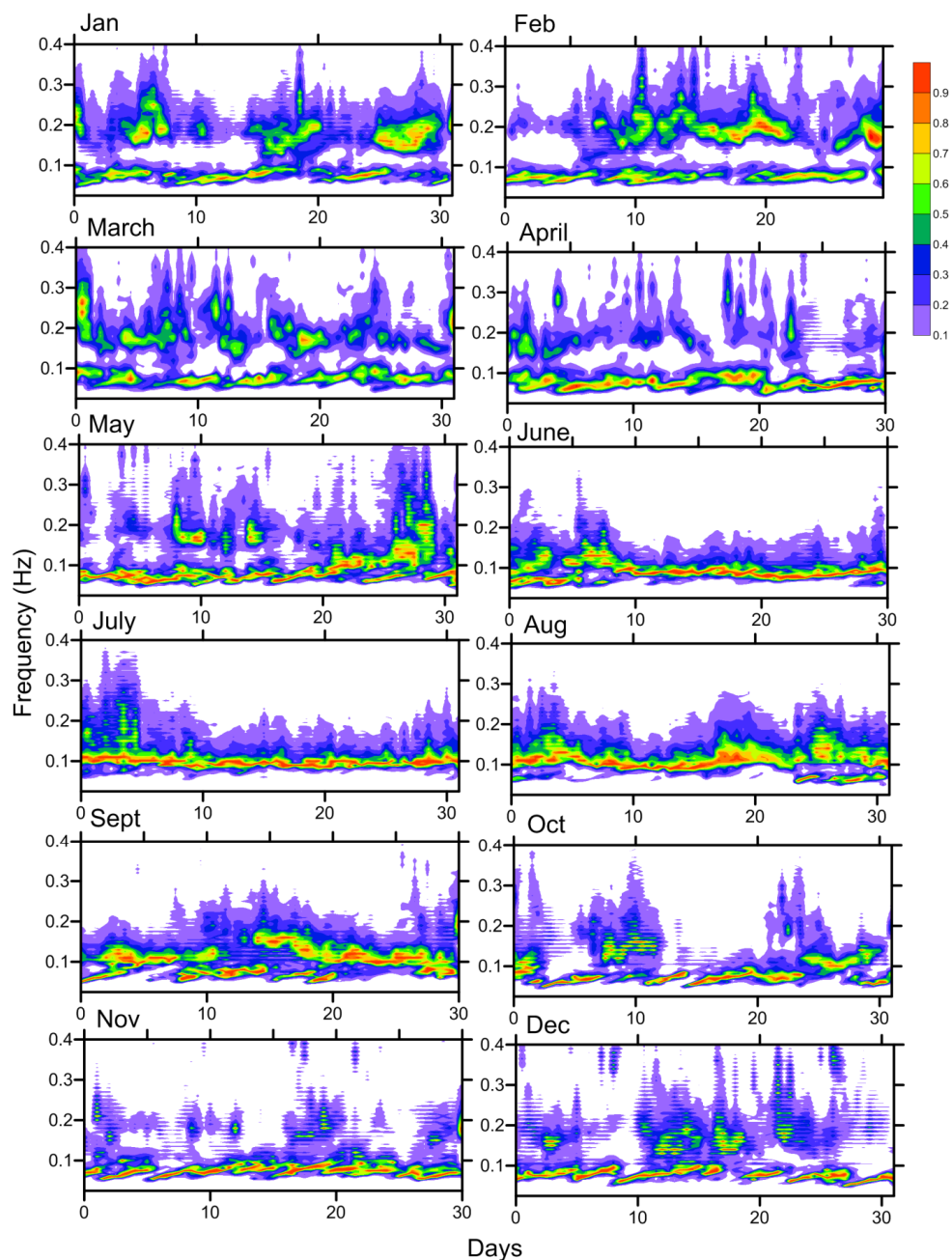


584
585

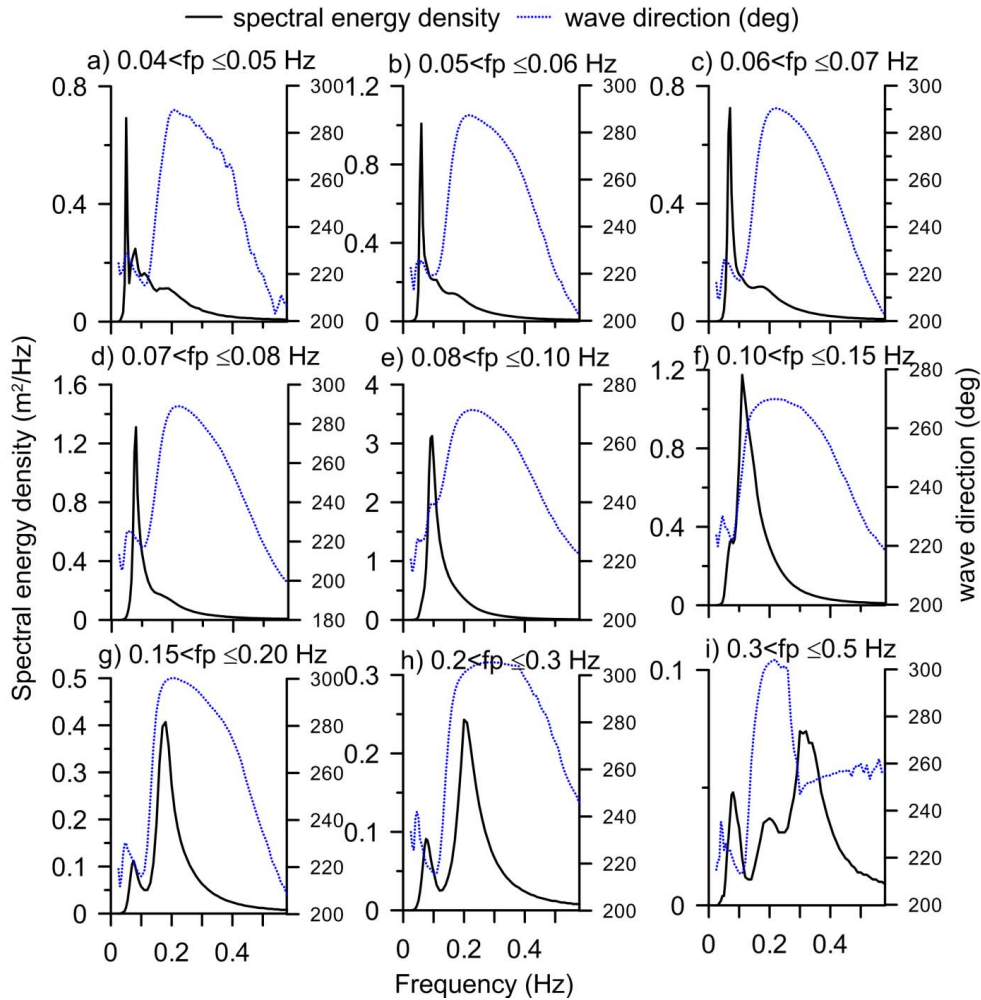
Figure 8. Monthly average wave direction at different frequencies in different months



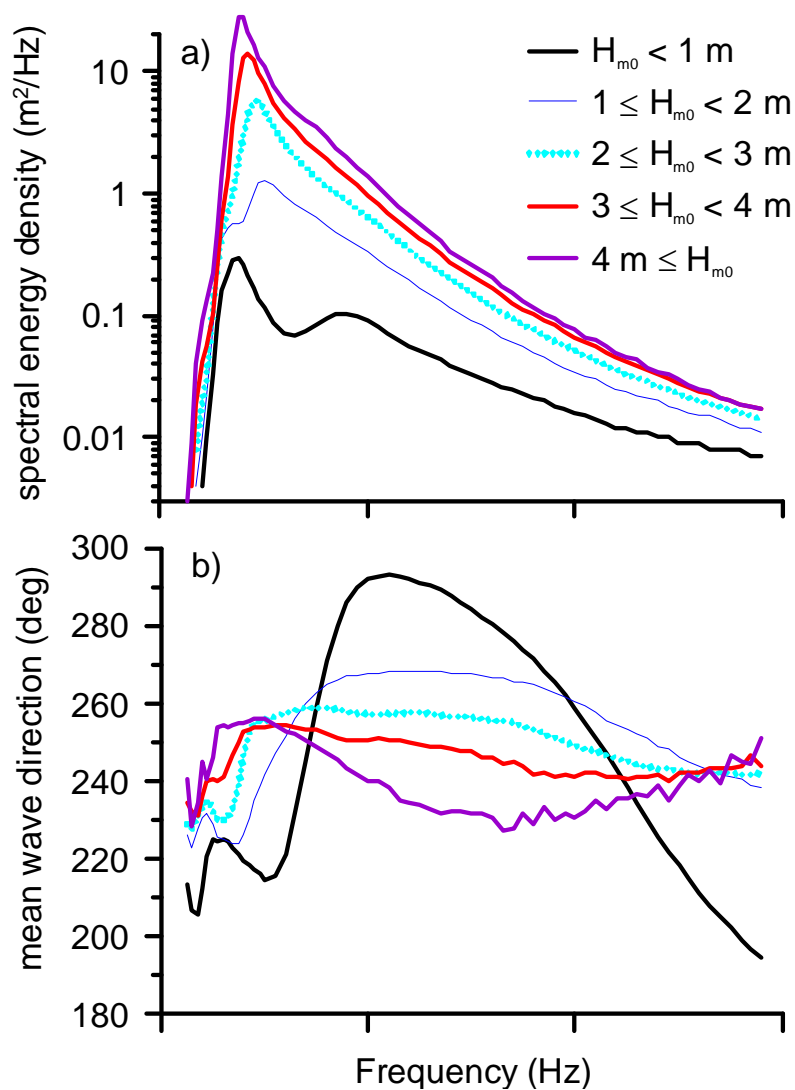
586



587
588 Figure 9. Temporal variation of normalized spectral energy density in different months (data from
589 2011 to 2015 used)

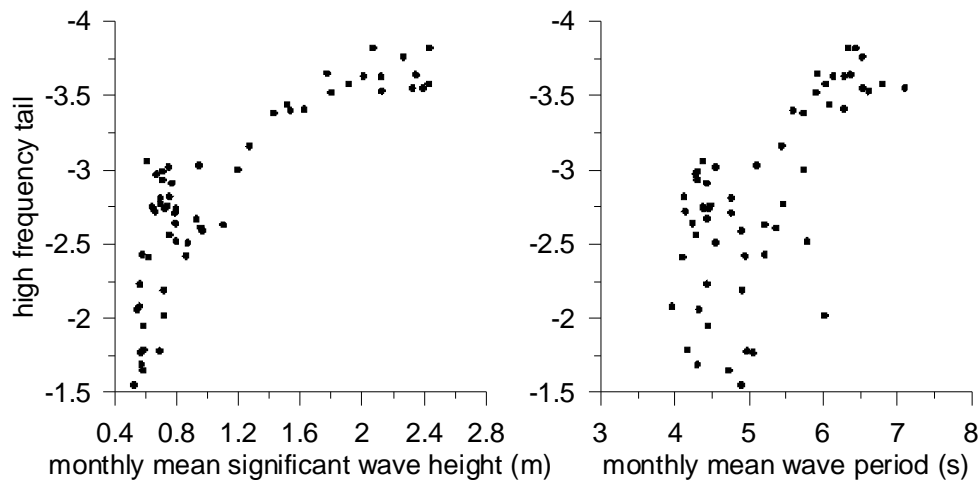


590
 591 Figure 10. Plot of average spectral energy density and average mean wave direction of waves
 592 grouped under different peak frequency bins



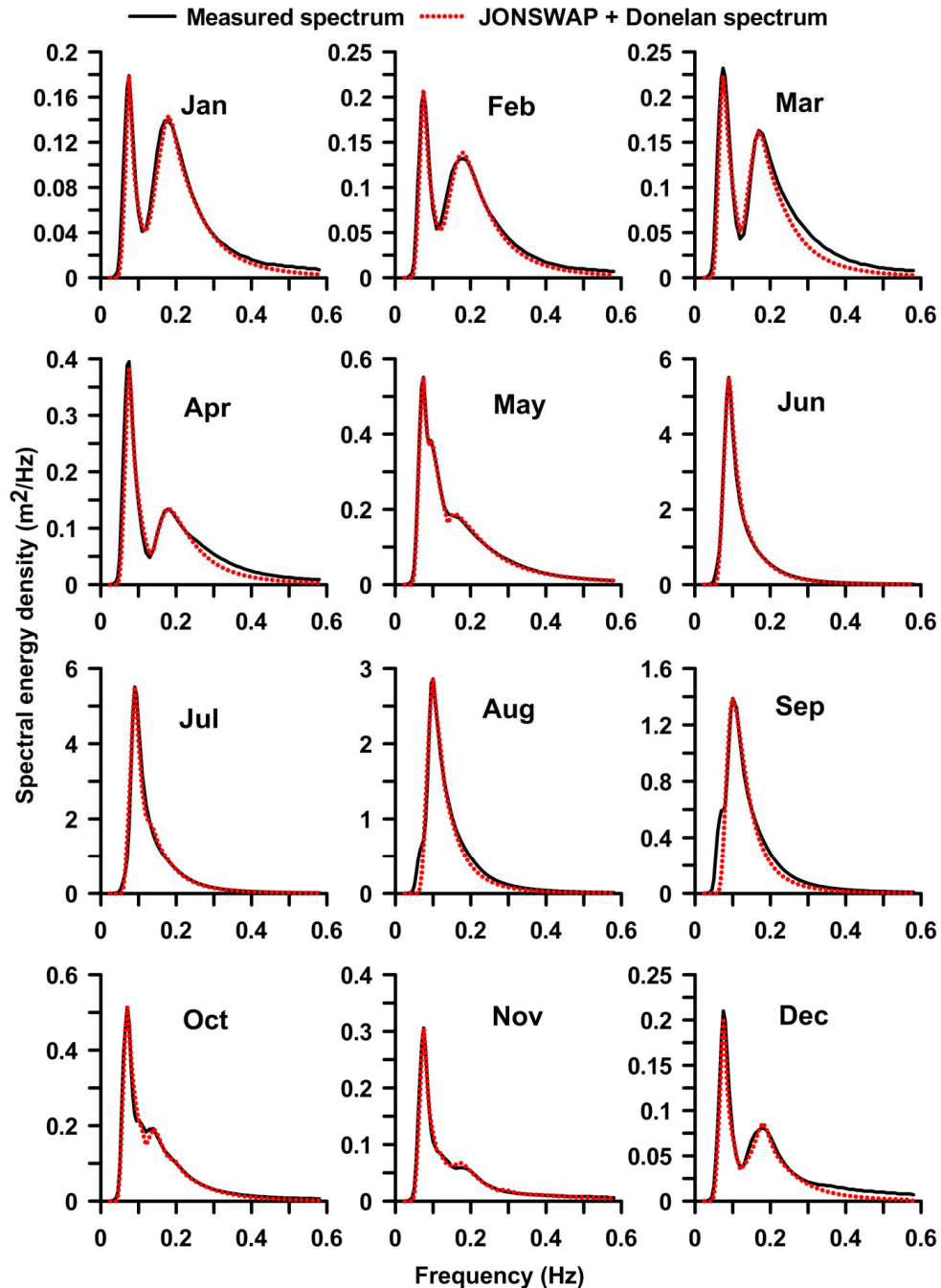
593
594
595
596

Figure 11. Plot of a) average spectral energy density and b) average mean wave direction of waves under different H_{m0} with frequency



597
598
599
600

Figure 12. Plot of high frequency tail with significant wave height (left panel) and with mean wave period (right panel)



601
602 Figure 13. Fitted theoretical spectra along with the monthly average wave spectra for different
603 month